

A Numerical Model for Atmospheric Icing of Conductor Bundles

Dipl.-Ing Tobias Wagner and Prof. Dr.-Ing. Udo Peil

International Graduate School of Risk Management of Natural Hazards, Institute of Steel Structures, TU Braunschweig, Beethovenstr. 51, 38106 Braunschweig, Germany, *t.wagner@tu-bs.de*

Abstract—This paper presents a numerical icing model simulating rime ice deposit on conductor bundles. Due to the assumptions made in the flow calculation existing numerical icing models are restricted to single cables. To overcome this restriction the Finite Element Method with a Reynolds Average Navier-Stokes (RANS) solver is used to calculate the incompressible and isothermal Navier-Stokes equation for a two-dimensional flow field. The closure problem of the RANS equations is addressed by a k - ϵ turbulence model. The fluid domain is discretized by a mapped boundary layer mesh in vicinity of the bodies in the stream and with a free mesh in the remaining domain. The multiphase flow of air and precipitation droplets is modelled with a Lagrangian approach, meaning that individual particle trajectories are computed. Any effect of the particles on the fluid flow is neglected. This one-way coupling of the fluid dynamics and the droplet motion is justified, since a low particle concentration in the flow is presumed. The particle trajectories are governed by Newton's second law, taking aerodynamic drag, gravity and buoyancy into consideration. The solver transfers this second order ordinary differential equation (ODE) into a pair of coupled first order ODE. These equations are then solved by a pair of four and five order Runge-Kutta algorithms. The particle trajectories provide the impinging location of the droplets on the cable or, respectively, the ice surface. The mass flux of icing particles can be visualised as stream tube reaching from the undisturbed flow to the surface, limited by the computed droplet trajectories. Within each tube the particles stream from the undisturbed flow to the surface, where the evolution of the ice front is determined. Hence, the ice accretion is calculated iteratively, accounting for geometrical changes due to ice deposit in the flow calculation.

I. NOMENCLATURE

A_p	particle cross-section [m ²]
\mathbf{a}_p	particle acceleration vector [m/s ²]
C_D	drag coefficient [-]
C_μ	model constant [-]
$C_{\epsilon 1}$	model constant [-]
$C_{\epsilon 2}$	model constant [-]
d_p	particle diameter [m]
\mathbf{e}_i	ice evolution vector [m]
\mathbf{F}	force vector [N]
\mathbf{g}	gravity vector [m/s ²]
k	turbulent kinetic energy [J/kg]
l	length along a flat plate [m]
LWC	liquid water content in the air [g/m ³]
MVD	medium volume diameter [μ m]
m_p	particle mass [kg]
p	pressure [N/m ²]
R	Macklin's Parameter [-]

Re	Reynolds number [-]
Re_p	particle Reynolds number [-]
Re_l	Reynolds number of a flat plate [-]
t	time [s]
t_{int}	time step of the icing model [s]
T_s	surface temperature [°C]
\mathbf{U}	average velocity vector [m/s]
\mathbf{u}	velocity vector [m/s]
\mathbf{u}_p	particle velocity vector [m/s]
u_0	free stream velocity [m/s]
$u_{p,0}$	particle velocity in the undisturbed flow [m/s]
u_{pi0}	particle impact velocity [m/s]
\mathbf{u}_{rel}	relative velocity vector [m/s]
V_p	particle volume [m ³]
α	collision efficiency [-]
α_i	particle impact angle [°]
β	collection efficiency [-]
χ	accretion efficiency [-]
δ	accretion rate [m]
δ_ν	depth of the viscous boundary layer [m]
ϵ	turbulent dissipation rate [m ² /s ³]
μ	dynamic viscosity of the fluid [Ns/m ²]
μ_T	turbulent viscosity of the fluid [Ns/m ²]
ν	kinematic viscosity of the fluid [m ² /s]
ρ_i	ice density [kg/m ³]
ρ_p	particle density [kg/m ³]
ρ_f	fluid density [kg/m ³]
σ_k	model constant [-]
τ	stress tensor [N/m]

II. INTRODUCTION

ATMOSPHERIC icing occurs when freezing raindrops, supercooled cloud droplets or snow flakes hit a surface. This phenomenon can cause significant damage to electric power transmission networks, especially in combination with wind. Therefore shape and density of ice forming on cables are of major interest in investigating the risk of failure. Large amplitude oscillations at low frequencies, or also twisting due to asymmetrical icing of cables, can cause fatigue damages. In extreme events atmospheric icing can cause severe damage on towers and power lines [1,2]. A large number of small-scale failures can cause enormous damage just as well as a single major winter storm event [3,4]. Examples of such events took place in northern America in 1998 and to a much smaller

extent in Germany in 2005, where the devastating power of winter storms left many people without electricity for weeks and caused significant monetary damage [5,6]. By causing cascading problems, with time black outs have major effects on telecommunication, transportation, money transfer and industrial production. Even essential needs like food supply and production and medical services are in danger after a certain period without electricity [7].

The following three reasons make it seem useful to develop a simulation scheme allowing for particle motion based on the stream occurring around conductor bundles: Firstly, meteorological observations from the 1950s give a first hint that tandem arrangements of cylinders have an effect on the icing process [8,9]. Secondly, the vulnerability of modern societies to blackouts is growing with the increasing demand of energy and increasing use of capacity. Since public authorities, in Germany for example, tend to restrict the construction of new transmission lines, bundled conductors are used increasingly to cope with the rising energy demand [10]. Thirdly, available numerical models are restricted to single cables due to the assumptions made in the air flow calculation [11,12,13,14,15,16]. A good overview of cable icing models and the mechanism of ice accretion is given by Poots [17] and by Makkonen and Lozowski [5,18].

Modelling atmospheric icing includes a computation of the mass flux of icing particles as well as a determination of the icing conditions: Icing conditions are defined by the heat balance on the ice surface. Messinger [19] proposed a basic scheme to investigate heat balances on ice surfaces. The icing condition influences the accretion mass and furthermore the evolving ice density. Three major types of deposit, namely rime, glaze and wet snow lead to significant loads on structures. For glaze ice and wet snow formation the heat balance on the ice surface is very important. It is termed as wet growth, because a liquid layer forms on the ice surface. In contrast to that, rime ice develops in dry growing conditions. The heat transfer within the system can be neglected, because the latent heat of the droplets released during freezing is dissipated without changing the state of the ice and the surface conditions, hence no liquid layer arises. Computation of the mass flux of icing particles is an important factor in the ice accretion. Shape and to a smaller extent also density of ice evolution are influenced by the characteristics of the particle trajectories.

The present work focuses on the mass flux of icing droplets and the formation of the ice front. In a first step, this model is limited to a dry ice growing regime, in other words, only rime ice evolution is considered. With further development the model is to include also wet ice conditions.

III. FLUID DYNAMIC MODEL

To calculate air flow around the conductors the finite element software COMSOL Multiphysics and a Reynolds Average Navier-Stokes (RANS) model are used [20]. The fluid dynamic calculation is based on the incompressible and isothermal Navier-Stokes equation. It assumes a constant

density and a constant temperature throughout the fluid domain. Hence, the conservation of mass becomes

$$\nabla \mathbf{u} = 0 \quad (1)$$

where \mathbf{u} is the velocity vector. Assuming the fluid to be Newtonian and adding the Stokes assumption the stress tensor becomes

$$\boldsymbol{\tau} = \mu \left(\nabla \mathbf{u} + (\nabla \mathbf{u})^T \right) \quad (2)$$

where μ is the dynamic viscosity. Therefore the conservation of momentum is

$$\rho \frac{\partial \mathbf{u}}{\partial t} + (\rho \nabla \mathbf{u}) \mathbf{u} = -\nabla p + \nabla \left(\mu \left(\nabla \mathbf{u} + (\nabla \mathbf{u})^T \right) \right) + \mathbf{F} \quad (3)$$

with ρ_f is the fluid density, p is the pressure and \mathbf{F} is the force vector acting on the body.

The conservation of energy is independent of the other two conservation equations, because density and temperature are assumed to be constant. Therefore it is not included in the flow calculation [21].

It is computational very expensive to resolve the smallest scales of a turbulent flow with an adequately fine mesh and time step. Using a coarser resolution leads to a closure problem of the equation. To solve the closure problem the time averaging by the RANS approach and a k - ϵ turbulence model is chosen [21]. In spite of its weakness in the pressure representation on body surfaces the k - ϵ model was preferred at this stage, because of its tendency to ease convergence. A k - ω turbulence model, known for its superior performance in external flow calculations, might be used in a later stage [22].

The model introduces the turbulent kinetic energy k and the dissipation rate of turbulence ϵ as independent variables. The closure problem is then solved using the turbulent viscosity, which is determined by

$$\mu_T = \rho C_\mu \frac{k^2}{\epsilon} \quad (4)$$

where $C_\mu = 0.09$ is a model constant. The turbulent kinetic energy k is derived from the Reynold stresses, which are expressed by

$$\begin{aligned} \rho \frac{\partial k}{\partial t} - \nabla \cdot \left(\left(\mu + \frac{\mu_T}{\sigma_k} \right) \nabla k \right) + \rho \mathbf{U} \cdot \nabla k \\ = \frac{1}{2} \mu_T \left(\nabla \mathbf{U} + (\nabla \mathbf{U})^T \right)^2 - \rho \epsilon \end{aligned} \quad (5)$$

where \mathbf{U} is the average velocity vector and the model constant $\sigma_k = 1.0$. The corresponding equation for ϵ can only be determined in a similar way when all terms that have no equivalent term in the equation for k are excluded. The equation is then defined as

$$\left(\left(\mu + \frac{\mu_T}{\sigma_\epsilon} \right) \nabla \epsilon \right) + \rho \mathbf{U} \cdot \nabla \epsilon \quad (6)$$

$$= \frac{1}{2} C_{\epsilon 1} \frac{\epsilon}{k} \mu_T \left(\nabla \mathbf{U} + (\nabla \mathbf{U})^T \right)^2 - \rho C_{\epsilon 2} \frac{\epsilon^2}{k}$$

where the model constants are $C_{\epsilon 1} = 1.44$, $C_{\epsilon 2} = 1.92$ and $\sigma_\epsilon = 1.3$. They are a commonly used set of model constants developed by Launder & Sharma and published in Wilcox [23]. One important assumption made by this turbulence model is that the equilibrium of turbulence is in boundary layers and therefore formation and dissipation of turbulences are equal. Since this is not always true, the spatial extension of recirculation zones is usually underestimated [20].

The extension of the recirculation zone is expected to have a significant influence on the ice formation process on the downstream cable. Therefore the simulation results can underestimate the influence of the wake on the downstream cable.

A. Solver

The equation system is solved by a segregated solver algorithm, where the variables are divided in groups. The velocity components and pressure compose the first group and the logarithm of turbulent kinetic energy and of turbulent dissipation rate are the second group. The linear system solver Pardiso is applied to each group [24,25]. It terminates, when the estimated error of both groups is smaller than the given tolerance [20]. The final error estimate of the results for both groups is $e < 0.001$.

The chosen linear system solver and their settings were examined along a test scheme of the DFG (German Research Foundation) [26]. The benchmark test investigates a 2D flow field passing a cylinder. It gives a feasible range for five parameters describing the flow field. In a stationary computation the aerodynamic lift and drag coefficient, the length of the recirculation zone, the pressure difference at the stagnation point and the subtending point in the wake are determined. In a transient calculation the maxima of lift and drag coefficient and in addition the Strouhal number are defined. The settings achieved the requirements satisfactorily.

B. Model Geometry and Boundary Conditions

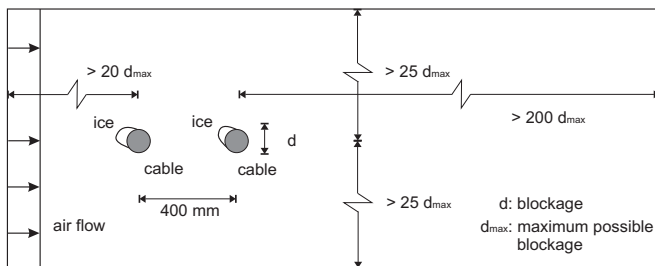


Fig. 1. Model Geometry

Figure 1 shows the model dimensions, which are chosen to provide enough clearance between the external boundaries and the iced cable. So that even for the largest possible blockage in the flow, the influence of the boundaries on flow around cable and ice body is irrelevant.

In contrast to investigations commonly undertaken in the field of aeroelasticity, the gravity needs to be included in the flow calculation to describe the particle motion correctly. Hence the boundary conditions need to balance the hydrostatic pressure. For this purpose pressure constrains are applied on vertices along the inlet and outlet boundary. At the inlet and outlet boundaries the velocity is set to be equal to the free stream velocity. Cable and ice surface are modelled as a solid wall, where the velocity profile at the cable and ice surface is described by the logarithmic wall function.

To develop an icing algorithm capable to simulate accretion on a conductor bundle, this investigation focuses on two cables in a tandem arrangement. If the algorithm proves successful for two cables, it can easily be applied to other bundle geometries with more cables.

Further bundle geometries will be investigated in the future. Power transmission lines are also constructed with bundles of three, four or even more cables [10].

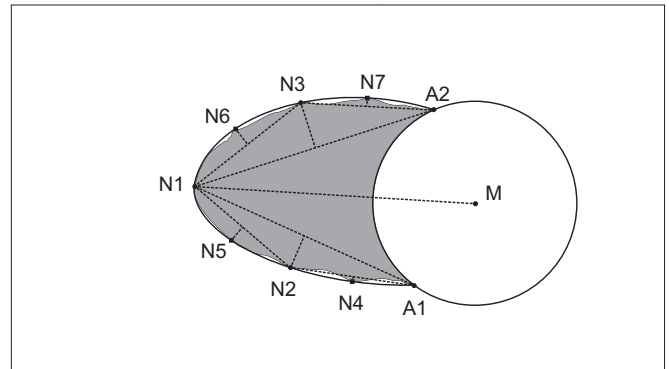


Fig. 2. Surface approximation algorithm evaluation the supporting points (N_i) with the contact points of ice and cable surface (A_1 and A_2) and centre of the cable (M).

The ice surface calculated by the icing model has often coarse uneven areas. Thus a fine resolution of the surface can lead to problems with the meshing algorithm and convergence of the solver. Resolving the coarse areas of the surface has only a small impact on the final result. Therefore an algorithm is developed to approximate the ice surface by splines to achieve geometry with continuous curvature. First, the centre of the cable (M), the contact points of the ice and cable surface (A_1 and A_2) and the point furthest away from the cable (N_1) are determined. Then the algorithm evaluates the distance between neighbouring points and between the connecting line and the ice surface. If one of these limits is exceeded, a new point (N_i) is inserted. The algorithm works also in case of a closed ice surface, where A_1 and A_2 are at identical coordinates. If the cable, due to weak torsional stiffness, rotates under the eccentric ice load during the icing process, the ice can grow around the entire circumference of the cable.

C. Mesh

The fluid domain is meshed with a free mesh. A boundary layer mesh is inserted at the cable surface or respectively the ice surface. The depth of the boundary layer mesh is chosen to be 1.5 times the depth of a boundary layer derived by an empirical equation for turbulent flows and flat plates [27].

$$\partial(l) = \frac{0.37l}{Re_l^{1/5}} \quad (7)$$

where l is half of the cable and ice body perimeter and Re_l is the Reynolds number

$$Re_l = \frac{u_0 l}{\nu} \quad (8)$$

where u_0 is the free stream velocity and ν is the kinematical viscosity.

Using wall functions on the surfaces leads to an additional requirement on the mesh. The boundary layer depth in viscous units should be in the range of $30 < y^+ < 300$ [20]. The value of y^+ depends on the dimensions of the boundary layer mesh. This requirement is fulfilled.

IV. PARTICLE TRAJECTORY CALCULATION

The Lagrangian approach is used to describe particle motion in the air flow, meaning that individual particle trajectories are modelled. This approach is used even though it does not provide information about the particle density in the flow field. Presuming a low particle concentration in the flow, decoupling of the flow and the trajectory calculation and neglecting any effect of the particles on the air flow is justified [28]. Consequently the mixed stream of air and precipitation droplets is modelled as a one-way coupled two-phase flow. The motion of the individual particles is described by Newton's second law. The solver rewrites this second order ordinary differential equation (ODE) into a pair of coupled first order ODE. A four and five order Runge-Kutta algorithms are used to solve two equations in each direction, one for velocity and one for spatial location [20].

The governing equation for the particle motion is given by

$$m_p \mathbf{a}_p = \sum \mathbf{F} \quad (9)$$

where m_p particle mass, \mathbf{a}_p particle acceleration and \mathbf{F} the sum of drag, buoyancy and gravity acting on the particle. Other forces acting on the particle are neglected and the particles are assumed to be spherical. Itemising the force vector leads to an expression for the aerodynamic drag force, depending on the relative velocity

$$\mathbf{u}_{rel} = \mathbf{u}_p - \mathbf{U} \quad (10)$$

where \mathbf{u}_p is the particle velocity vector. Furthermore we need an expression for the force due to density differences of particle and fluid. The equation can then be written as

$$m_p \mathbf{a}_p = -C_D A_p \frac{\rho_f}{2} |\mathbf{u}_{rel}| \cdot \mathbf{u}_{rel} - \rho_f V_p \mathbf{g} + \rho_p V_p \mathbf{g} \quad (11)$$

with C_D the drag coefficient, A_p the cross-section and V_p the volume of the particle, ρ_p is the particle density and \mathbf{g} the gravity vector.

In order to rearrange equation 11, the particle Reynolds number is introduced as

$$Re_p = \frac{|\mathbf{u}_{rel}| d_p \rho_f}{\mu}, \quad (12)$$

where d_p is the droplet diameter. Now equation 11 can be written as

$$m_p \mathbf{a}_p = -\frac{C_D Re_p}{24} \cdot 3\pi d_p \mu \cdot \mathbf{u}_{rel} + (\rho_p - \rho_f) \cdot \frac{\pi d_p^3}{6} \cdot \mathbf{g} \quad (13)$$

where ρ_p is the particle density. To solve the equation, the relation of C_D and Re_p needs to be defined. For $Re_p \ll 1$, C_D is given by the Stokes's law. When Re_p increases empirical equations need to be applied. Based on experiments by Langmuir and Boldgett [29] the following set of equations is proposed.

$$\frac{C_d Re_p}{24} = 1 - 0.391 \cdot Re_p^{0.3289} + 0.5648 \cdot Re_p^{0.4561} \quad (14)$$

for $0 < Re_p \leq 10$

$$\frac{C_d Re_p}{24} = 1 + 0.1767 \cdot Re_p^{0.6536} \quad (15)$$

for $10 < Re_p \leq 200$

$$\frac{C_d Re_p}{24} = 4.001 - 0.01052 \cdot Re_p^{1.048} \quad (16)$$

for $200 < Re_p$

The experiments by Langmuir and Blodgett cover a wide range of particle Reynolds numbers. Regarding transmission line icing only the range of low Re_p is important. Therefore the formulae presented here are designed to fit best low Re_p . The equations have a coefficient of determination of over 99% for $Re_p < 2000$. Beyond this range the accuracy decreases only slightly.

The distribution of droplet diameters in natural precipitation is not uniform. It can be described by droplet spectra. Calculating the motion for every single droplet diameter occurring in a given precipitation is computationally expensive. But in the scope of transmission line icing it is possible to deduce the behaviour of the whole spectrum from the motion of a droplet of medium volume diameter (MVD), with sufficient accuracy [16].

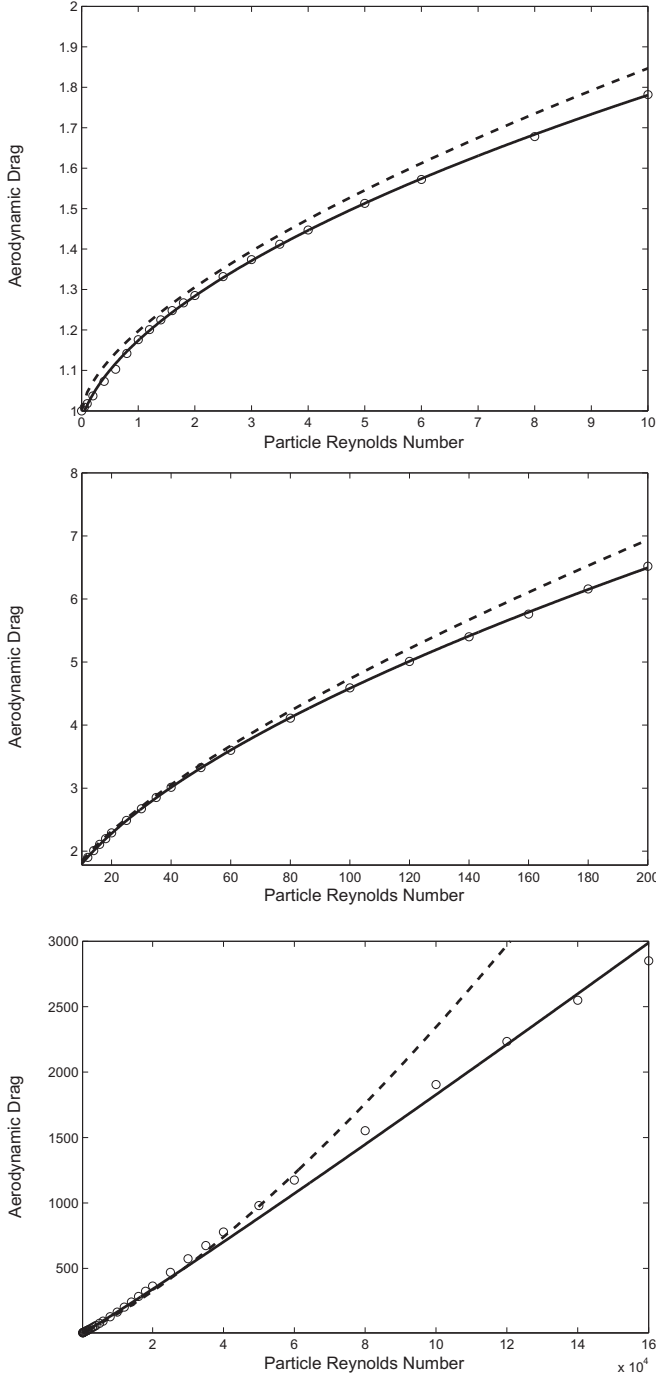


Fig. 3. Experimental results (\circ) and an empirical equation (---) published by Langmuir and Blodgett [29] are compared with the proposed approximation (—) of the aerodynamic drag ($C_D Re_p / 24$) for Reynolds numbers of spherical particle (Re_p).

V. ICE EVOLUTION MODEL

The impinging locations of the particle trajectory determine mass flux calculation of icing particles on the surface. The mass flux can be visualised as a stream tube starting from the undisturbed flow to the surface, limited by the computed droplet trajectories. Within each tube the particles stream from the undisturbed flow towards the surface. Once the particle flux is given, the computation of the ice evolution can start.

The implementation of the icing model follows the fundamental mechanism illustrated by Diem [8] and Makkonen [5]. In order to represent the program structure, the notation and the arrangement of the equations are different. The ice growth is expressed by a vector normal to the surface. It includes four parameters, namely collection, catch and accretion efficiency. The fourth parameter is termed accretion rate and states the maximal growth rate under the given conditions during one time step.

The local collision efficiency is the ratio of droplet mass flux in the undisturbed incoming flow to mass flux of droplets impinging on the surface.

$$\alpha = \frac{A_0}{A_i} \quad (17)$$

where A_0 is the initial trajectory spacing in the undisturbed flow and A_i is the corresponding spacing of the impinging location on the surface. In case of freezing rain the calculation leads to $\alpha \approx 1$.

For rime ice accretion due to in-cloud icing the collection efficiency is assumed to be

$$\beta = 1 \quad (18)$$

In case of freezing rain collection efficiency is calculated as proposed by Poets [17]

$$\beta = \cos(\alpha_i) \quad (19)$$

where α_i is the impact angle of the droplets. Rime ice accretion due to both in-cloud and freezing rain lead to streamlined ice deposit. In-cloud icing conditions lead to decreasing α freezing rain to decreasing β towards the edges. However one can regard the product of both as catch efficiency.

The accretion efficiency accounts for particles that hit the surface, but do not freeze and are either enclosed unfrozen in the deposit or leave the surface due to wind drag and gravity. Since only rime ice accretion is considered here and all impinging particles freeze instantly, the accretion efficiency is

$$\chi = 1 \quad (20)$$

In order to define the ice accretion ratio the ice density is determined by empirical equations. Following the investigation of Fu, Farzaneh and Bouchard [30] the equations derived by Bain and Gayet [31] where chosen.

$$\begin{aligned} \rho_i &= 110 \cdot R^{0.76} & \text{for } 0 < R \leq 10 \\ \rho_i &= \frac{R}{R + 5.61} \cdot 10^3 & \text{for } 10 < R \leq 60 \\ \rho_i &= 917 & \text{for } 60 < R \end{aligned} \quad (21)$$

Macklin's Parameter is [32]

$$R = \frac{MVD \cdot u_{p,i}}{2 \cdot T_s} \quad (22)$$

where MVD is the medium volume diameter, $u_{p,i}$ is the impact speed and T_s is the surface temperature. In conjunction with the liquid water content (LWC) in the air the ice accretion ratio

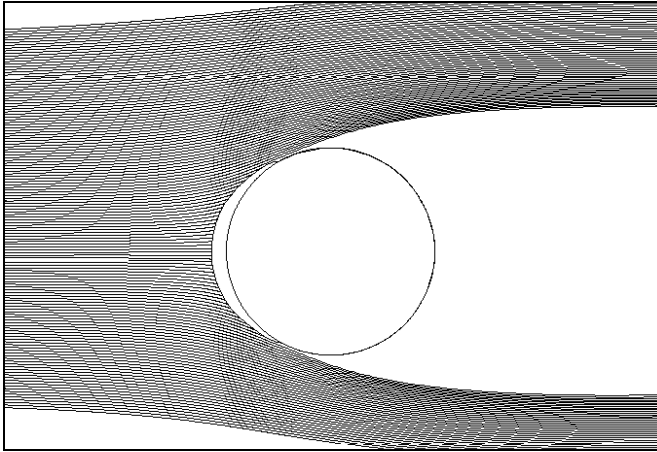


Fig. 3. Particle trajectories and ice deposit on upstream cable in a tandem arrangement with a horizontal spacing of $s=0.4m$. Simulation parameters are wind velocity $u=5m/s$, particle diameter $MVD=28\mu m$, ambient temperature $T_a=-15^\circ C$ and cable diameter $d=40mm$.

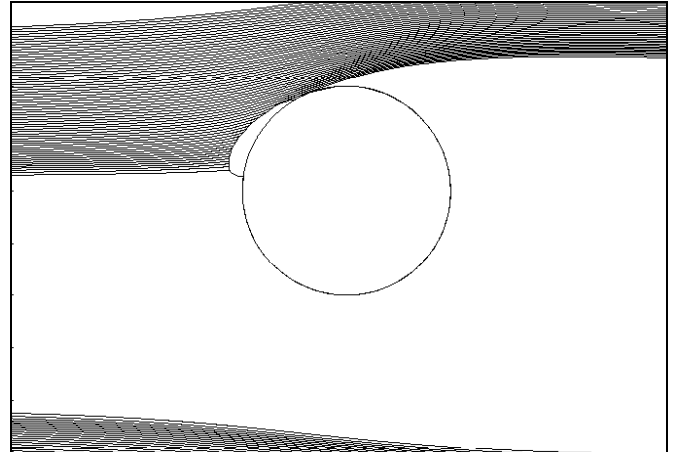


Fig. 4. Particle trajectories and ice deposit on downstream cable in a tandem arrangement with a horizontal spacing of $s=0.4m$. Simulation parameters are wind velocity $u=5m/s$, particle diameter $MVD=28\mu m$, ambient temperature $T_a=-15^\circ C$ and cable diameter $d=40mm$.

is given by

$$\delta = \frac{LWC \cdot u_{p,0} \cdot t_{int}}{\rho_i} \quad (23)$$

The ice front growth along the vector is then expressed in

$$e_i = \alpha \cdot \beta \cdot \chi \cdot \delta \cdot n \quad (24)$$

where $u_{p,0}$ is the particle velocity in the undisturbed flow, t_{int} is the time interval of ice evolution with unchanged flow field and n is the vector normal to the surface. On the basis of the new ice geometry a new simulation step is started.

In order to verify the model, two test cases for rime ice accretion on single cables due to in-cloud icing were simulated. The test cases consist of numerical and experimental results published by Fu, Farzaneh and Bouchard [30]. Over all the comparison showed satisfying results [33]. But further comparison with experimental findings especially of conductor icing experiments should be done in the future.

VI. ACKNOWLEDGMENT

The authors thankfully acknowledge the support of the German Research Foundation (DFG) given to the International Graduate School 802, Risk Management of Natural and Civilisation Hazards on Buildings and Infrastructure.

VII. REFERENCES

- [1] Bendel, W. B., Paton, D., "A review on the effect of ice storms on the power industry", *Journal of Applied Meteorology*, vol. 20, pp. 1445-1449, 1981.
- [2] Jones, K. F., "An evaluation of the severity of the January 1998 ice storm in northern New England", Technical Report for FEMA Region 1, 1998.
- [3] Llinca, A., Llinca, F., Ignat, I., "Numerical study of iced conductors aerodynamics", in *Proc. 1996 7th International Workshop on Atmospheric Icing of Structures*.
- [4] Muhlerin, N. D., "Atmospheric icing and communication tower failure in the United States", *Cold Regions Science and Technology*, vol. 27, pp. 91-104, 1998.
- [5] Makkonen, L., "Models for the growth of rime, glaze, icicles and wet snow on structures", *Phil. Trans. R. Soc. London*, vol.358, pp. 2913-2939, 2000.
- [6] Bundesnetzagentur, "Über die Versorgungsstörung im Netzgebiet des RWE im Münsterland vom 25.11.2005", Bundesnetzagentur für Elektrizität, Gas, Untersuchungsbericht Telekommunikation Post und Eisenbahnen, 2006.
- [7] Bundesamt für Bevölkerungsschutz und Katastrophenhilfe, "Zusammenfassung der Katastrophenübung LÜKEX 2004", 2006. [unpublished]
- [8] Diem, M., "Höchstlasten der Nebelfrostablagerungen an Hochspannungsleitungen", *Archiv für Meteorologie, Geophysik und Bioklimatologie B7*, pp. 87-95, 1955.
- [9] Waibel, K., "Die meteorologischen Bedingungen für Nebelfrostablagerungen an Hochspannungsleitungen im Gebirge", *Archiv für Meteorologie, Geophysik und Bioklimatologie B3*, S. 74-83, 1955.
- [10] Kiebling, F., Nefziger, P. & Kaintzyk, U., *Freileitungen: Planung, Berechnung, Ausführung*, Springer, 2001.
- [11] Lozowski, E. P., Stallabrass, J. R., Hearty, P. F., "The icing of an unheated non-rotating cylinder Part I: A simulation model", *Journal of Climate and Applied Meteorology*, vol. 22, pp. 2053-2074, 1983.
- [12] Makkonen, L., "Modelling of ice accretion on wires", *Journal of Climate and Applied Meteorology*, vol. 23, pp. 929-939, 1984.
- [13] Makkonen, L., "Estimation of wet snow accretion on structures", *Cold Regions Science and Technology*, vol. 17, 83-88, 1989.
- [14] Makkonen, L., "Modeling power line icing in freezing precipitation", *Atmospheric Research*, vol. 46, pp. 131-142, 1998.
- [15] Jones, K. F., "A simple model for freezing rain ice loads", *Atmospheric Research*, vol. 46, pp. 87-97, 1998.
- [16] Fu, P., "Modelling and simulation of the ice accretion process on fixed or rotating cylindrical objects by boundary element method", PhD Thesis University of Quebec 2004.
- [17] Poots, G., *Ice and snow accretion on structures*, Research Studies Press LTD, 1996.
- [18] Lozowski, E., Makkonen, L., "Fifty years of progress in modelling the accumulation of atmospheric ice on power network equipment", in *Proc. 2005 11th International Workshop on Atmospheric Icing of Structures*.
- [19] Messinger, B. L., "Equilibrium temperature of an unheated icing surface as a function", *Journal of the Aeronautical Sciences*, vol. 20, pp. 29-41, 1953.
- [20] COMSOL AB, "Heat Transfer and Chemical Engineering Model User Guide for Comsol Multiphysics", COMSOL AB, 2007.
- [21] Zienkiewicz, O. C., Taylor, R. L., Nithiaparsu, P., *The Finite Element Method for Fluid Dynamics*, Elsevier Butterworth-Heinemann, 2005.
- [22] Schlichting, H., Gersten K., *Grenzschicht-Theorie*, Springer, 2006.
- [23] Wilcox, D. C., *Turbulence modelling for CFD*, DCW Industries, 1998.

- [24] Schenk, O., Gärtner, K., "Solving Unsymmetric Sparse Systems of Linear Equations with PARDISO", *Journal of Future Generation Computer Systems*, vol. 20(3), pp. 475-487, 2004.
- [25] Schenk, O., Gärtner, K., "On fast factorization pivoting methods for symmetric indefinite systems", *Elec. Trans. Numer. Anal.*, vol. 23, pp. 158-179, 2006.
- [26] Schäfer, M., Turek, "Benchmark Computations of Laminar Flow Around a Cylinder", *Flow Simulation with High-Performance Computers*, vol. 52, pp. 547-566, 1996.
- [27] Anderson, J. D., *Computational Fluid Dynamics*, McGraw-Hill 1995.
- [28] Crowe, C., T., *Multiphase Flow Handbook*, CRC Press Inc. Taylor & Francis Group, 2006.
- [29] Langmuir, I., Blodgett, K.B., "A Mathematical Investigation of Water Droplet Trajectories", AAF Technical Report 5418, 1946.
- [30] Fu, P., Farzaneh, M., Bouchard, G., "Two-dimensional modelling of the ice accretion process on transmission line wires and conductors", *Cold Regions Science and Technology*, vol. 46, pp. 132-146, 2006.
- [31] Bain, M., Gayet, J. F., "Contribution to the modelling of the ice accretion process: Ice density variation with the impact surface angle", *Annals of Glaciology*, vol. 4, pp. 19-23, 1982.
- [32] Macklin, W. C., "The density and structure of ice formed by accretion", *Quarterly Journal of the Royal Meteorological Society*, vol. 88, pp. 30-50, 1962.
- [33] Wagner, T., Peil, U., Borri, C., "Numerical investigation of conductor bundle icing", in *Proc. 2009 5th European and African Conference on Wind Engineering*.